

# **Compressed lead-based perovskites reaching optimal Shockley-Queisser bandgap with prolonged carrier lifetime**

Gang Liu<sup>1,2\*</sup>, Lingping Kong<sup>1,2</sup>, Jue Gong<sup>3</sup>, Wenge Yang<sup>1,2</sup>, Ho-kwang Mao<sup>1,2\*</sup>, Zhenxian Liu<sup>2</sup>,  
Richard D. Schaller<sup>4</sup>, Dongzhou Zhang<sup>5</sup>, and Tao Xu<sup>3\*</sup>

<sup>1</sup>Center for High Pressure Science and Technology Advanced Research, Shanghai 201203, China.

<sup>2</sup>Geophysical Laboratory, Carnegie Institution of Washington, Washington, DC 20015, USA.

<sup>3</sup>Department of Chemistry and Biochemistry, Northern Illinois University, DeKalb, IL 60115, USA.

<sup>4</sup>Center for Nanoscale Materials, Argonne National Laboratory, Argonne, IL 60439, USA.

<sup>5</sup>Hawai'i Institute of Geophysics and Planetology, School of Ocean and Earth Science and Technology,  
University of Hawai'i at Manoa, Honolulu, HI 96822, USA.

\*e-mail: [liugang@hpstar.ac.cn](mailto:liugang@hpstar.ac.cn); [mao@gl.ciw.edu](mailto:mao@gl.ciw.edu); [txu@niu.edu](mailto:txu@niu.edu)

**Crystalline structure of materials plays a decisive role in light-matter interaction. Yet, despite its unprecedented progress, further efficiency boost of lead-based organic-inorganic perovskite solar cells is hampered by their greater bandgap than the optimum value according to Shockley-Queisser limit.<sup>1-11</sup> Here, we report the experimental achievement on the bandgap narrowing in formamidinium lead triiodide ( $\text{HC}(\text{NH}_2)_2\text{PbI}_3$ ) from 1.489 eV to 1.337 eV by modulating the lattice constants with modest hydraulic pressure up to 2.1 GPa, for the first time reaching the optimized bandgap for lead-based perovskites single-junction solar cells. Strikingly, such bandgap narrowing is accompanied with doubled carrier lifetime, and the enhancement in narrowed bandgap can be partially retained after the release of pressure. This work opens a new dimension in basic science understanding of structural photonics and paves an alternative pathway towards more efficient photovoltaic materials synthesis.**

The efficiency improvements of the emerging organic-inorganic lead triiodide ( $\text{CH}_3\text{NH}_3\text{PbI}_3$ ) perovskite solar cells have been quickly approaching the theoretical ceiling based on the material bandgap of 1.5-1.6 eV.<sup>1-7</sup> According to Shockley-Queisser theory, the efficiency limit for single-junction semiconductor-based solar cells under AM1.5 solar spectrum and one-Sun illumination is 33.7%, which requires a corresponding optimum bandgap energy of 1.34 eV,<sup>8-11</sup> much smaller than that of pristine  $\text{CH}_3\text{NH}_3\text{PbI}_3$ .<sup>12</sup> Efforts to tune the bandgap by chemical modifications lead to unwanted shorter carrier lifetime (substitution of Pb by Sn<sup>13,14</sup>) and/or larger bandgaps (substitution of I by Cl and/or Br<sup>15,16</sup>). Therefore, a pressing need is to explore an alternative way with fundamental understanding to narrow the bandgap while retaining, if not improving, the desirable photovoltaic merits of lead-based perovskites, particularly their long charge carrier lifetime that is crucial to their striking long carrier diffusion lengths.<sup>17-20</sup> By applying controllable

hydrostatic pressure on methylammonium lead trihalide ( $\text{CH}_3\text{NH}_3\text{PbX}_3$ ,  $\text{X}=\text{I}^-$  or  $\text{Br}^-$ ) perovskites, previous effort was able to narrow the material bandgaps through pressure-induced shrinkage in X-Pb-X bond lengths, but only for small extents before detrimental phase transition occurred,<sup>21-23</sup> thereby making the approach of optimum bandgap still an basic science challenge. One key atomic-level understanding of the interplay between bandgap and lattice structures is the Pb-I-Pb bond angles. Previous work indicates that the Pb-I-Pb in  $\text{CH}_3\text{NH}_3\text{PbI}_3$  only aligned linearly along one dimension, thus, the compression causes inhomogeneous contraction of Pb-I-Pb in three dimensions, which eventually leads to detrimental bond angle variation, i.e. phase transition was triggered at above 0.3 GPa.<sup>22,23</sup> Thus, seeking another Pb-based perovskite with linear Pb-I-Pb bonds along all three dimensions may bring about persistent bandgap narrowing under pressure while still keeping the attractive long carrier lifetime. Structurally analogous to  $\text{CH}_3\text{NH}_3\text{PbI}_3$ ,  $\text{HC}(\text{NH}_2)_2\text{PbI}_3$  (FAPbI<sub>3</sub>) composes of larger organic cation,  $\text{HC}(\text{NH}_2)_2^+$ , with cationic charge distributed over its structure via the  $\pi$  system. As such, it may stretch and flatten out the kinked Pb-I-Pb bonds along the other two dimensions, as suffered by  $\text{CH}_3\text{NH}_3\text{PbI}_3$ . Plus, it has demonstrated comparable device efficiency and optoelectronic properties to those of  $\text{CH}_3\text{NH}_3\text{PbI}_3$ .<sup>24-27</sup> Therefore, it is intriguing to study the properties of this material under elevated pressures. Herein, we report a striking bandgap narrowing of FAPbI<sub>3</sub> from 1.489 eV to 1.337 eV when applied pressure is increased from 1 atm to 2.1 GPa. This is the first report on reaching the optimal Shockley-Queisser bandgap in lead-based hybrid perovskites. An exceptional merit is that the narrowed bandgap is accompanied with carrier lifetime prolongation. Moreover, the narrowed bandgap formed under high pressure condition is partially retainable after pressure is released back to 1 atm, revealing insightful interplay between the lattice structure and photonic properties in the materials. This work could substantially resolve the mechanistic foundation of

hybrid lead halide perovskites and provide theoretical guidelines as well as engineering routes to significantly advance photovoltaic technology.

We performed high resolution synchrotron X-ray diffraction (XRD) to examine the crystal structure of the as-prepared FAPbI<sub>3</sub> samples. Results showed good fit between observed pattern and calculated result using trigonal *P3m1* model, as evidenced by the tiny discrepancy factors ( $R_p=1.17\%$ ,  $R_{wp}=2.42\%$  see Fig. 1a). Crystal lattice parameters were resolved to be  $a = b = 9.0001 \text{ \AA}$ ,  $c = 11.0726 \text{ \AA}$ ,  $\alpha = 90^\circ$ ,  $\gamma = 120^\circ$ , in good agreement with reports on trigonal FAPbI<sub>3</sub> ( $\alpha$ -FAPbI<sub>3</sub>).<sup>27-29</sup> It was previously discovered that optical bandgaps of hybrid halide perovskite materials are pressure-dependent.<sup>21-23</sup> In short, a redshift in bandgap with no less than 1.5 eV can be observed under mild pressure (<0.3 GPa), above which a phase transition occurs and the bandgap rebounds up. Surprisingly, however, the bandgap of  $\alpha$ -FAPbI<sub>3</sub> experienced a red-shift from 1.489 eV to 1.337 eV as hydrostatic pressure was increased from 1 atm to 2.1 GPa, reaching the Shockley-Queisser optimum bandgap for the first time for lead-based hybrid perovskites (see Figs. 1b-1e, Supplementary Note 1, and Supplementary Figs. S1-S11). Shockingly, the magnitude of change in bandgap (0.15 eV) is significantly greater than MAPbI<sub>3</sub> (0.04 eV) and MAPbBr<sub>3</sub> (0.03 eV),<sup>22,23</sup> as summarized in Fig. 1f.

To investigate the root course of the gigantic red-shift found in  $\alpha$ -FAPbI<sub>3</sub>, we conducted *in-situ* synchrotron high pressure XRD experiments up to 7.0 GPa at ambient temperature (Fig. 2). Fig. 2a shows the typical XRD patterns of FAPbI<sub>3</sub> as a function of pressure. For the first test pressure at 0.4 GPa, crystal structure can be readily resolved using ambient phase with space group *P3m1*, as supported by the refinement with relative small errors of  $R_p$  (1.05%) and  $R_{wp}$  (1.55%) (Supplementary Fig. S12). As pressure increases to 7.0 GPa, all XRD peaks of the continuously shifted to larger 2 theta (smaller *d*-spacing) range, while no new peak was observed.

All patterns are consistent with the  $P3m1$  structure and representative GSAS refinements results are listed in Supplementary Table 1. Although the absence of crystal phase transition was demonstrated, for the pressure higher than 2.5 GPa, anisotropic peak broadening was observed upon pressure increase, and broad background originated from the diffuse scattering appeared, suggesting the occurrence of amorphization associated with significantly distorted  $\text{PbI}_6$  octahedra. It is well known that the Pb-I-Pb bond angle represents the  $\text{PbI}_6$  octahedral tilting, which is responsible for the changes in the electronic structure close to the band edges, thus determines the band gap. For low-pressure phase  $P3m1$ , the Pb-I-Pb bond angle remains at nearly  $180^\circ$  along all three dimensions and the bond length shortens as the pressure increases (Fig. 2b). The essence of electron-photon interaction in hybrid lead iodide mainly involves the transition of electrons from the I  $5p$  states to the Pb  $6p$  states and a small quantity of localized transition from Pb  $6s$  to Pb  $6p$ . The former transition does not incur change of angular momentum quantum number, while the latter transition does not incur change of principal quantum number. Upon compression the atomic distance decreases, leading to enhanced overlapping between I  $5p$  and Pb  $6p$  orbitals. Such coupling between bonded electrons pushes up the valence band maximum (VBM). In contrast, the conduction band minimum (CBM) is mostly a nonbonding localized state of Pb  $p$  orbitals which is relatively insensitive to bond length or pressure. The net result, therefore, is the decrease in bandgap under pressures. However, as the pressure increases above 2.5 GPa, amorphization occurs, appearing as the XRD peaking broadening attributed to the distortion of the Pb-I-Pb bond. As such, the off-aligned Pb-I-Pb bond leads to less overlapping between the Pb  $s$  and I  $p$  orbitals, and consequently results in the widened bandgap (Supplementary Figs. S13-S15).

Notably, the absence of crystal phase transition in  $\text{FAPbI}_3$  under pressure plays a pivotal role

in an aggressive bandgap narrowing that reaches the optimal Shockley–Queisser bandgap for single-junction photovoltaic materials, as it allows a continuous bond length shrinkage (causing more overlapping between I  $5p$  and Pb  $6p$ ) without bond angle distortion (causing less overlapping between I  $5p$  and Pb  $6p$ ) prior to amorphization. Unlike methylammonium organic-inorganic perovskites, in which the Pb-I-Pb bond angle is aligned as nearly  $180^\circ$  only along one dimension, all the three Pb-I-Pb bond angles in  $\alpha$ -FAPbI<sub>3</sub> (trigonal  $P3m1$  space group) exhibit  $\sim 180^\circ$  (Fig. 2b). The minimized PbI<sub>6</sub> octahedra tilting of  $\alpha$ -FAPbI<sub>3</sub> can also be evidenced by its smaller bandgap than MAPbI<sub>3</sub> through greater steric size of FA<sup>+</sup> according to studies.<sup>29-31</sup> Spatially, the responses of the Pb-I-Pb bonds in FAPbI<sub>3</sub> to compression are similar and quasi-homogeneous. Then, a rational mechanistic understanding is that when all bond angles maintain  $\sim 180^\circ$ , as in the case of FAPbI<sub>3</sub>, the crystal undergoes a uniform compression that allows all atoms in the PbI<sub>6</sub> octahedral to remain their relative position to others, avoiding some preferential Pb-I-Pb bond bending (causing phase transition) as in the case of MAPbI<sub>3</sub> where  $I4/mcm$  to  $Imm2$  phase transition occurs at very mild pressure  $\sim 0.4$  GPa). Therefore, we believe it is the linear Pb-I-Pb geometry extending across whole Pb-I framework that functions to withstand dislocation between Pb and I, and thereby postponing the occurrence of structural phase transition. Additionally, compared to MA cations, higher probability of forming hydrogen bonds between FA cations may also contribute to the structural stability of FAPbI<sub>3</sub> under pressure.

On the other hand, the highly compressible nature of FAPbI<sub>3</sub> crystal is demonstrated by refinements on XRD patterns (Fig. 2a), which yields the relative changes of lattice constants and volume, as shown in Figs. 2c-2e. Compared to methylammonium organic-inorganic perovskites including MAPbI<sub>3</sub> (Supplementary Fig. S16), MASnI<sub>3</sub>,<sup>32</sup> and MAPbBr<sub>3</sub>,<sup>33</sup> lower bulk modulus

$K_0$  was observed in FAPbI<sub>3</sub>, being on the order of 11.0(2) GPa (Figs. 2f-2g). Such a soft characteristic results in an effective electron orbitals overlapping even at very low pressures, thus significant bandgap narrowing can be expected. In comparison to the rigid C-N bond in MAPbI<sub>3</sub>, the bendable V-shaped N-C-N bond in FAPbI<sub>3</sub> allows flexible space needed for achieving high compressibility (Supplementary Figs. S17-S18). Indeed, the smallest bulk modulus ( $K_0=8.0(7)$  GPa) was observed also in another formamidinium organic-inorganic hybrid iodide, namely, FASnI<sub>3</sub>.<sup>32</sup>

We further conducted static and dynamic *in-situ* high pressure photoluminescence (PL) measurements on FAPbI<sub>3</sub> to examine the pressure dependence of carrier lifetime (Fig. 3), a decisive quantity for attaining the near-bandgap photovoltage and for the solar cell device performance.<sup>6,19,20</sup> The defect-related trap states in MAPbI<sub>3</sub> are believed to be located in shallower levels close to band edges, thus the electron-hole pair recombination is easily prohibited.<sup>34-35</sup> Compared to MAPbI<sub>3</sub>, FAPbI<sub>3</sub> exhibits shorter carrier lifetime,<sup>36</sup> suggesting higher trap density and/or deeper trap levels.<sup>37</sup> As the bandgap narrows under compression (Fig. 1), the previously deep states become relatively closer to band edges, i.e. shallower traps, leading to longer carrier lifetime. Fig. 3a and its inset show the pressure-driven evolutions of the static PL spectrum and the main PL peak position, respectively. The pronounced red-shift of PL peak position from 810 nm at ambient condition to 872 nm at 2.4 GPa is in agreement with the observed trend of bandgap narrowing upon compression. For dynamic (time resolved) PL measurements, the data were measured at the wavelength of respective main static PL peaks. Our high pressure PL and time resolved PL measurement was carried out on the same piece of polycrystalline sample in compression to exclude the various defect states among different samples. PL time decay traces at various pressures were collected in Figs. 3b-3f and all time-

resolved traces were fitted by biexponential decay function  $I_{\text{PL}}(t) = I_{\text{int}}[\alpha \cdot \exp(-t/\tau_1) + \beta \cdot \exp(-t/\tau_2)] + I_0$  to quantify the PL decay dynamics, where the slow component  $\tau_1$  and the fast component  $\tau_2$  are assigned to free carrier recombination in the bulk and on the surface, respectively. At ambient pressure, FAPbI<sub>3</sub> sample has a superposition of slow and fast dynamics, being the order of 125 ns and 25 ns (Fig. 3b), respectively. Interestingly, both slow and fast components exhibit an obvious rise in compression. At 1.7 GPa, the carrier lifetime reaches a “peak” value of 284 ns (Figs. 3e and 3g), over two times longer than that at ambient pressure. As the applied pressure further increased to 2.4 GPa, a dramatic decrease in carrier lifetime was observed, which can be attributed to the fact that greater defective states were generated at higher pressures due to the emergence of amorphization. At every tested pressure, the relative contribution of the slow component to the static PL amounts to a stable value of over 77% (Fig. 3h), thus the pressure-driven carrier lifetime prolongation is a bulk-related intrinsic phenomenon. Taking the account of the relative contribution of the slow and fast components, we evaluated the mean carrier lifetime  $\langle\tau\rangle$  defined as  $[\alpha\tau_1/(\alpha\tau_1+\beta\tau_2)]\tau_1 + [\beta\tau_2/(\alpha\tau_1+\beta\tau_2)]\tau_2$ , and an increase in  $\langle\tau\rangle$  of over 70% was achieved at 1.7 GPa (Fig. 3i and Supplementary Table S2).

To seek the potential usefulness of the pressure-induced bandgap narrowing for practical applications, we investigated the retainability of the narrowed bandgap after pressure is completely released (Figs. 4a-4c). By subtracting the measured transmission spectra (see Fig. 4a) of the silicon oil background from that of the decompressed FAPbI<sub>3</sub> sample (in silicon oil) from 7.1 GPa to 1 atm, the absorbance and transmittance spectra of the sample were obtained, as shown in Fig. 4b. Clearly, sharp absorbance and transmittance onsets are presented around 870 nm. By extrapolating the linear portion of the  $(adh\nu)^2$  versus photonic energy  $h\nu$ , a direct

bandgap of 1.447 eV was estimated for the decompressed sample, which is 42 meV lower than that before compression (1.489 eV, see Fig. 1b). To explore the structural origin of such enhanced optical property, we compared the XRD patterns before compression and after decompression for the same FAPbI<sub>3</sub> sample. Echoing the bandgap, the crystal structure also exhibits a partial retainable behavior, as evidenced by the fact that all XRD peaks shifted to larger 2 theta range after the pressure is released (Fig. 4d). Correspondingly, for decompressed sample the lattice constants and volume were estimated to be  $a = 8.9809 \text{ \AA}$ ,  $c = 10.98576 \text{ \AA}$ , and  $V = 767.33993 \text{ \AA}^3$ , obviously smaller than those in sample before compression ( $a = 9.00001 \text{ \AA}$ ,  $c = 11.07269 \text{ \AA}$ , and  $V = 776.70601 \text{ \AA}^3$ ) (Fig. 4e), meaning the structural information at high pressure is memorized by the sample after pressure is released. Therefore, the retainability of bandgap narrowing from high pressure condition can be readily understood by the observed structural plasticity of FAPbI<sub>3</sub>, namely, the non-reversible lattice shrinkage in response to the applied pressure.

This study unprecedentedly achieved the optimal Shockley-Queisser bandgap in organic-inorganic lead trihalide perovskites using a clean physical tool, i.e. compression, and revealed key fundamental mechanics that governs the structural photonics in hybrid perovskite materials. More strikingly, two benign phenomena are accompanied with the narrowed bandgap, including the elongated carrier lifetime and the partial retainability of the narrowed bandgap after pressure is released. Our discovery suggest that pressure is an effective tool to tune the photonic properties of materials by modulating their lattice structure in a precise and controllable manner, thus to achieve better materials-by-design for various photovoltaic and optoelectronic systems.

## References

1. Burschka, J. *et al.* Sequential deposition as a route to high-performance perovskite-sensitized solar cells. *Nature* **499**, 316-319 (2013).
2. Im, J-H., Jang, I-H., Pellet, N., Grätzel, M. & Park N-G. Growth of  $\text{CH}_3\text{NH}_3\text{PbI}_3$  cuboids with controlled size for high-efficiency perovskite solar cells. *Nature Nanotech.* **9**, 927-932 (2014).
3. Kaltenbrunner, M. *et al.* Flexible high power-per-weight perovskite solar cells with chromium oxide-metal contacts for improved stability in air. *Nature Mater.* **14**, 1032-1039 (2015).
4. Green, M. A., Ho-Baillie, A. & Snaith, H. J. The emergence of perovskite solar cells. *Nature Photon.* **8**, 506-514 (2014).
5. Jeon, N. J. *et al.* Solvent engineering for high-performance inorganic-organic hybrid perovskite solar cells. *Nature Mater.* **13**, 897-903 (2014).
6. Nie, W. *et al.* High-efficiency solution-processed perovskite solar cells with millimeter-scale grains. *Science* **347**, 522-525 (2015).
7. Chen, W. *et al.* Efficient and stable large-area perovskite solar cells with inorganic charge extraction layers. *Science* **350**, 944-948 (2015).
8. Nozik, A. J. Photovoltaics: separating multiple excitons. *Nature Photon.* **6**, 272-273 (2012).
9. Shockley, W. & Queisser, H. J. Detailed balance limit of efficiency of p-n junction solar cells. *J. Appl. Phys.* **32**, 510-519 (1961).
10. Sha, W. E. I., Ren, X., Chen, L. & Choy, W. C. H. The efficiency limit of  $\text{CH}_3\text{NH}_3\text{PbI}_3$  perovskite solar cells. *Appl. Phys. Lett.* **106**, 221104 (2015).
11. Saidaminov, M. I., Abdelhady, A. L., Maculan, G. & Bakr, O. M. Retrograde solubility of formamidinium and methylammonium lead halide perovskites enabling rapid single crystal growth. *Chem. Commun.* **51**, 17658-17661 (2015).

12. Li, F. *et al.* Ambipolar solution-processed hybrid perovskite phototransistors. *Nat. Commun.* **6**, 82338 (2015).
13. Hao, F., Stoumpos, C. C., Cao, D. H., Chang, R. P. H. & Kanatzidis, M. G. Lead-free solar-state organic-inorganic halide perovskite solar cells. *Nature Photon.* **8**, 489-494 (2014).
14. Parrott, E. S. *et al.* Effect of structural phase transition on charge-carrier lifetimes and defects in  $\text{CH}_3\text{NH}_3\text{SnI}_3$  perovskite. *J. Phys. Chem. Lett.* **7**, 1321-1326 (2016).
15. Brenner, T. M., Egger, D. A., Kronik, L., Hodes, G. & Cahen, D. Hybrid organic-inorganic perovskites: low-cost semiconductors with intriguing charge-transport properties. *Nat. Rev. Mater.* **1**, 15007 (2016).
16. Luo, B. *et al.* Organolead halide perovskite nanocrystals: branched capping ligands control crystal size and stability, *Angew. Chem. Int. Ed.* **55**, accept, (2016). DOI: 10.1002/anie.201602236.
17. Stranks, S. D. *et al.* Electron-hole diffusion lengths exceeding 1 micrometer in an organometal trihalide perovskite absorber. *Science* **234**, 341-344 (2013).
18. Xing, G. *et al.* Long-range balanced electron and hole-transport lengths in organic-inorganic  $\text{CH}_3\text{NH}_3\text{PbI}_3$ . *Science* **342**, 344-347 (2013).
19. Shi, D. *et al.* Low trap-state density and long carrier diffusion in organolead trihalide perovskite single crystals. *Science* **347**, 519-522 (2015).
20. Wehrenfennig, C., Eperon, G. E., Johnston, M. B., Snaith, H. J. & Herz, L. M. High charge carrier mobilities and lifetimes in organolead trihalide perovskites. *Adv. Mater.* **26**, 1584-1589 (2014).

21. Wang, Y. *et al.* Pressure-induced Phase transformation, reversible amorphization, and anomalous visible light response in organolead bromide perovskite. *J. Am. Chem. Soc.* **137**, 11144-11149 (2015).
22. Jiang, S. *et al.* Pressure-dependent polymorphism and band-gap tuning of methylammonium lead iodide perovskite. *Angew. Chem. Int. Ed.* **55**, 6540-6544 (2016).
23. Jaffe, A., *et al.* High-pressure single-crystal structures of 3D lead-halide hybrid perovskites and pressure effects on their electronic and optical properties. *ACS Cent. Sci.* **2**, 201-209 (2016).
24. Lee, J-W., Seol, D-J., Cho, A-N. & Park, N-G. High-efficiency perovskite solar cells based on the black polymorph of  $\text{HC}(\text{NH}_2)_2\text{PbI}_3$ . *Adv. Mater.* **26**, 4991-4998 (2014).
25. Zhumekenov, A. A. *et al.* Formamidinium lead halide perovskite crystals with unprecedented long carrier dynamics and diffusion length. *ACS Energy Lett.* **1**, 32-37 (2016).
26. Eperon, G. E. *et al.* Formamidinium lead trihalide: a broadly tunable perovskite for efficient planar heterojunction solar cells. *Energy Environ. Sci.* **7**, 982-988 (2014).
27. Pang, S. *et al.*  $\text{NH}_2\text{CH}=\text{NH}_2\text{PbI}_3$ : An alternative organolead iodide perovskite sensitizer for mesoscopic solar cells. *Chem. Mater.* **26**, 1485-1491 (2014).
28. Stoumpos, C. C., Malliakas, C. D. & Kanatzidis, M. G. Semiconducting tin and lead iodide perovskites with organic cations: phase transitions, high mobilities, and near-infrared photoluminescent properties. *Inorg. Chem.* **52**, 9019-9038 (2013).
29. Amat, A. *et al.* Cation-induced band-gap tuning in organohalide perovskites: interplay of spin-orbit coupling and octahedra tilting. *Nano Lett.* **14**, 3608-3616 (2014).
30. Filip, M. R., Eperon, G. E., Snaith, H. J. & Giustino, F. Steric engineering of metal-halide perovskites with tunable optical band gaps. *Nat. Commun.* **5**, 5757 (2014).

31. Lee, J. H., Lee, J-H., Kong, E-H. & Jang, H. M. The nature of hydrogen-bonding interaction in the prototypic hybrid halide perovskite, tetragonal  $\text{CH}_3\text{NH}_3\text{PbI}_3$ . *Sci. Rep.* **6**, 21687 (2016).
32. Lee, Y., Mitzi, D. B., Barnes, P. W., & Vogt, T. Pressure-induced phase transitions and templating effect in three-dimensional organic-inorganic hybrid perovskites. *Phys. Rev. B* **68**, 020103(R) (2003).
33. Swainson, I. P., Tucker, M. G., Wilson, D. J., Winkler, B., & Milman, V. Pressure response of an organic-inorganic perovskite: Methylammonium lead bromide. *Chem. Mater.* **19**, 2401-2405 (2007).
34. Johnston, M. B. & Herz, L. M. Hybrid perovskites for photovoltaics: charge-carrier recombination, diffusion, and radiative efficiencies. *Acc. Chem. Res.* **49**, 146-154 (2016).
35. Yin, W-J., Shi, T. & Yan, Y. Unusual defect physics in  $\text{CH}_3\text{NH}_3\text{PbI}_3$  perovskite solar cell absorber. *Appl. Phys. Lett.* **104**, 063903 (2014).
36. Han, Q. et al. Single crystal formamidinium lead iodide (FAPbI<sub>3</sub>): Insight into the structural, optical, and electrical properties. *Adv. Mater.* **28**, 2253-2258 (2016).
37. Yin, W-J., Yang, J-H., Kang, J., Yan, Y. & Wei, S-H. Halide perovskite materials for solar cells: a theoretical review. *J. Mater. Chem. A* **3**, 8926-8942 (2015).

## **Acknowledgments**

G.L., L.K., W.Y. and H-k.M. acknowledge the support from NSAF (Grant No. U1530402). T.X. acknowledges the support from the U.S. National Science Foundation (CBET-1150617). High pressure powder structure characterizations were performed at beamline 16-BM-D at HPCAT, Advanced Photon Source (APS), Argonne National Laboratory. HPCAT operations are supported by DOE-NNSA under Award No. DE-NA0001974 and DOE-BES under Award No. DE-FG02-99ER45775, with partial instrumentation funding by the National Science Foundation (NSF). Part of this work was also performed at the Center for Nanoscale Materials (CNM), Argonne National Laboratory, and the Infrared Lab of the National Synchrotron Light Source (NSLS II), Brookhaven National Laboratory (BNL). The use of APS and CNM facilities was supported by the U. S. Department of Energy, Office of Science, Office of Basic Energy Sciences (DE-AC02-06CH11357). The Infrared Lab was supported by National Science Foundation (EAR 1606856, COMPRES) and DOE/NNSA (DE-NA-0002006, CDAC). We also thank Dr. Victor V. Ryzhov for his experimental support.

## **Author contributions**

G.L. and L.K. carried out the experiments and analyzed the data. J.G. synthesized samples. W.Y., Z.L., R.D.S., and D.Z. contributed materials analysis tools. G.L. and T.X. conceived the idea. G.L., J.G., and T.X. wrote the manuscript. All authors contributed to the revision of the manuscript. H-k.M. is responsible for overall direction and coordination.

## **Competing financial interests**

The authors declare no competing financial interests.

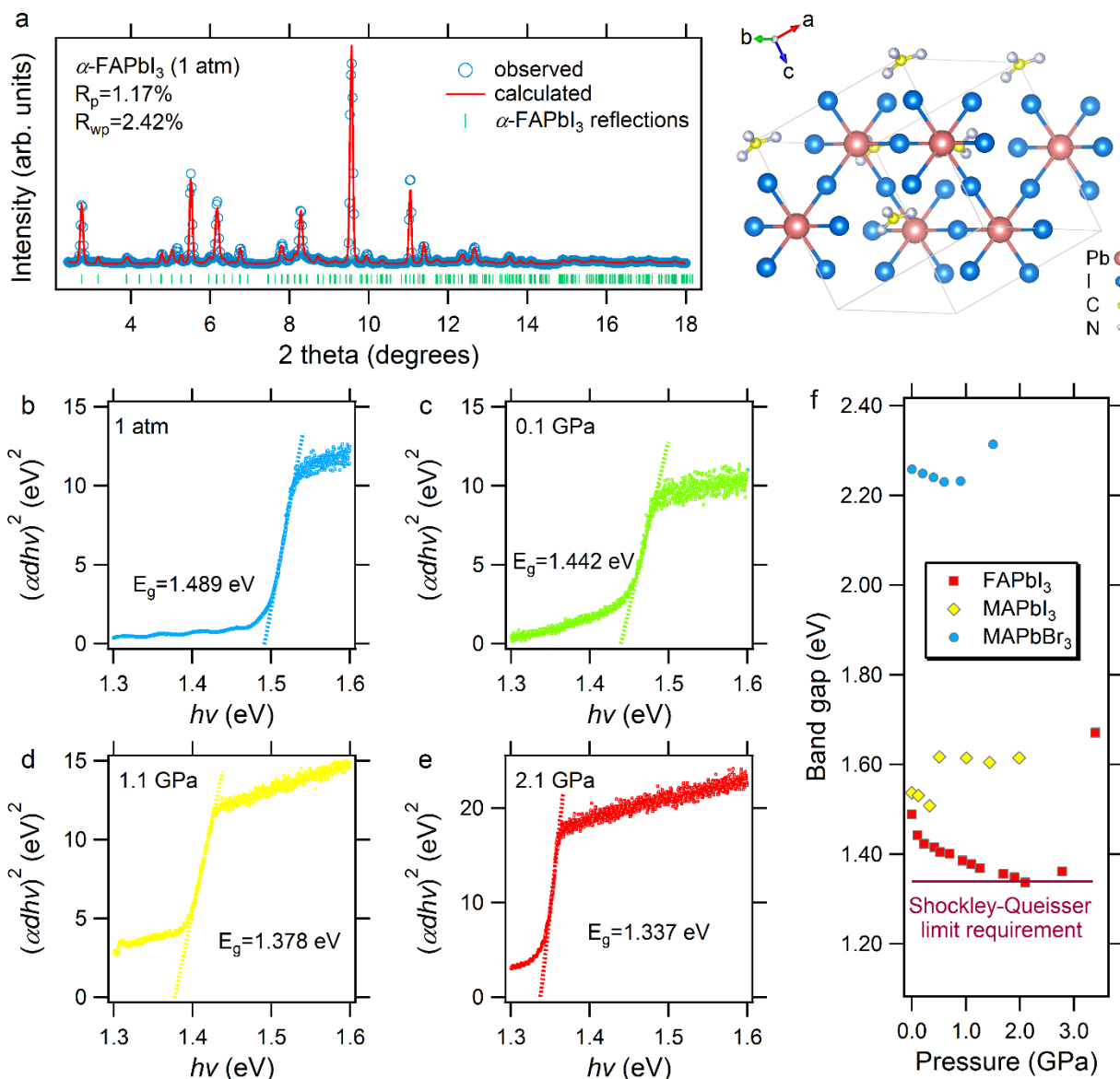


**Figure 1. Direct experimental evidence of bandgap narrowing down to Shockley-Queisser optimal magnitude in compressed FAPbI<sub>3</sub>.** **a**, high-resolution synchrotron XRD pattern measured at ambient condition (1 atm) for as-prepared FAPbI<sub>3</sub> sample. The crystal structure can be well fitted using trigonal  $\alpha$ -FAPbI<sub>3</sub> structure with  $P3m1$  space group symmetry (blue open circle: experimental data; red line: calculated result; green bar: Bragg reflections of  $\alpha$ -FAPbI<sub>3</sub>). Schematic crystal structure of trigonal  $\alpha$ -FAPbI<sub>3</sub> is also shown here. **b-e**, direct bandgap Tauc

plots of  $\alpha$ -FAPbI<sub>3</sub> collected at 1 atm, 0.1 GPa, 1.1 GPa, and 2.1 GPa, respectively. Magnitudes of bandgaps can be estimated by extrapolating the linear portion of the Tauc plots to the baselines. Pressure-induced red-shift of the band gap gradually occurs from 1 atm up to 2.1 GPa, where the smallest magnitude 1.337 eV was observed, reaching the Shockley-Queisser optimal bandgap (1.34 eV). **f**, pressure-dependent optical bandgap evolutions of FAPbI<sub>3</sub> (red), MAPbI<sub>3</sub> (yellow) and MAPbBr<sub>3</sub> (blue). The symbol size covers the size of the error bars.

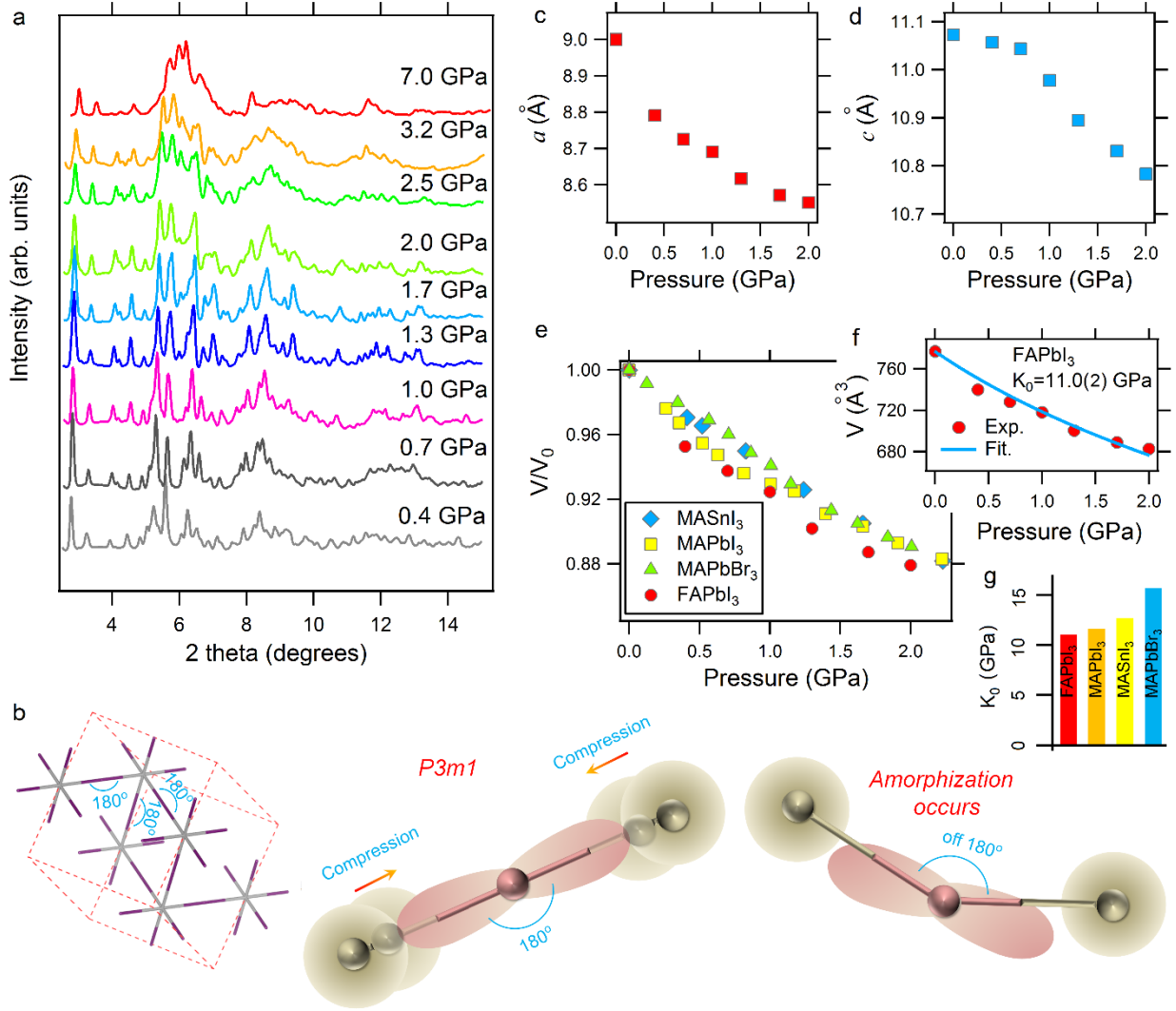


**Figure 2. Pressure-induced structural evolution of FAPbI<sub>3</sub>.** **a**, pressure dependent *in-situ* synchrotron angle dispersive X-ray diffraction patterns of FAPbI<sub>3</sub> in compression up to 7.0 GPa. The absence of crystal phase transition before amorphization is concluded since no new peak can be identified. **b**, Pb-I inorganic framework of trigonal α-FAPbI<sub>3</sub>, from which three dimensional ~180° Pb-I-Pb bond angles are highlighted. The schematic models of the red-shift and blue jump are shown. For the trigonal *P3m1* phase, as pressure increases the Pb-I-Pb bond angles maintain 180° three-dimensionally and the electron wave function overlaps more, pushing VBM up and narrowing bandgap. When amorphization occurs, the Pb-I-Pb bond angle becomes much smaller

than  $180^\circ$  and the electron wave function overlaps much less. The purple and grey shadows denote the electronic clouds of I  $5p$  and Pb  $6p$ , respectively. **c** and **d**, pressure dependence of lattice constants  $a$  and  $c$  for  $\alpha$ -FAPbI<sub>3</sub> unit cell. **e**, pressure dependence of relative changes in lattice volume of MASnI<sub>3</sub> (blue), MAPbI<sub>3</sub> (yellow), MAPbBr<sub>3</sub> (green) and FAPbI<sub>3</sub> (red). Compared to methylammonium organic-inorganic perovskites, FAPbI<sub>3</sub> exhibits higher compressibility. The bulk modulus  $K_0$  of FAPbI<sub>3</sub> was estimated to be 11.0(2) GPa by fitting experimental data with the Birch relation  $P(V) = \frac{3}{2} B_0 [(\frac{V_0}{V})^{\frac{7}{3}} - (\frac{V_0}{V})^{\frac{5}{3}}] \{1 + \frac{3}{4} (B' - 4) [(\frac{V_0}{V})^{\frac{2}{3}} - 1]\}$ , where we assume  $B' = 4$  (**f**). In **c-f**, the symbol size covers the size of the error bars. **g**. comparison of  $K_0$  values among FAPbI<sub>3</sub> (red), MAPbI<sub>3</sub> (orange), MASnI<sub>3</sub> (yellow) and MAPbBr<sub>3</sub> (blue).

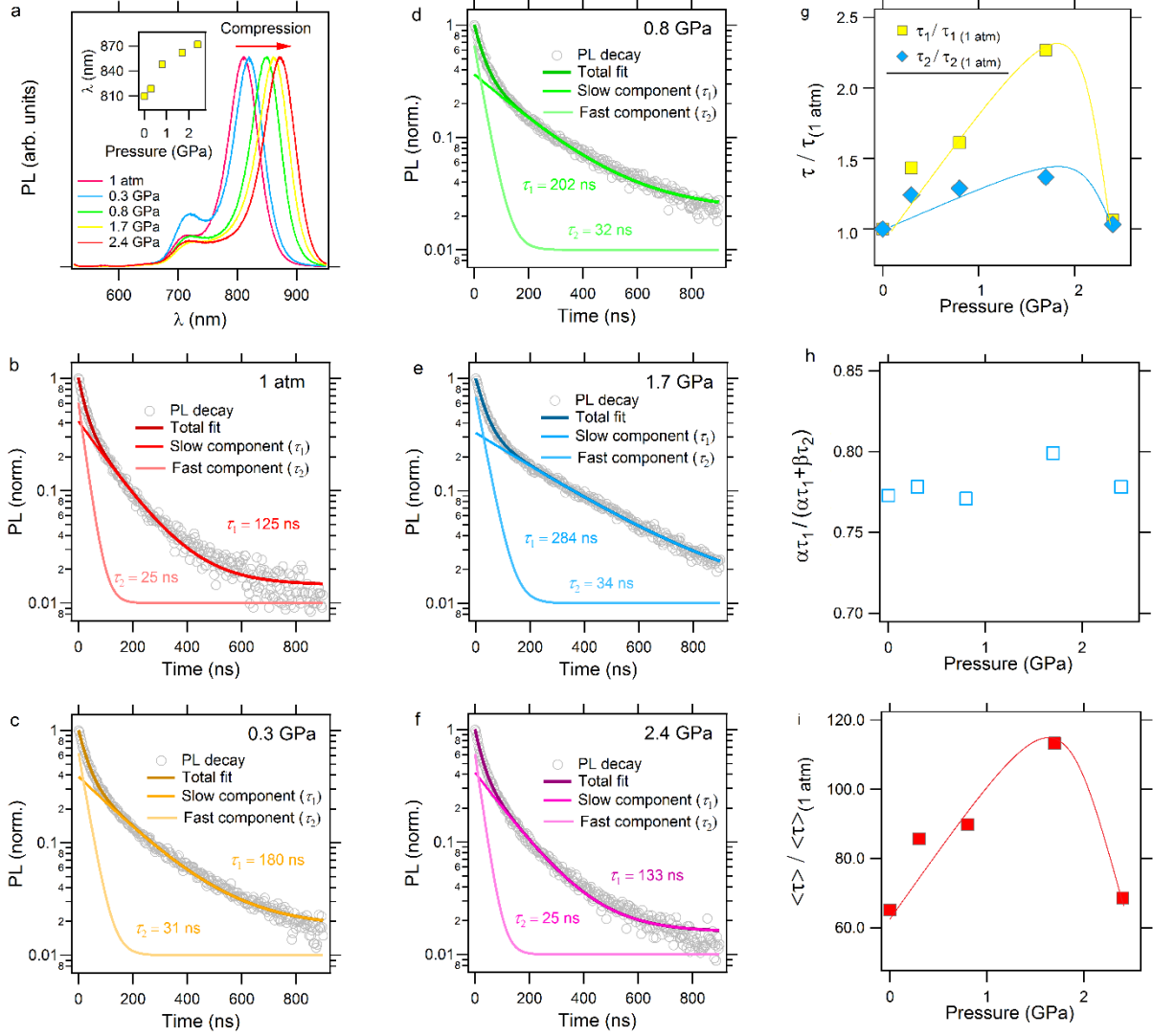


**Figure 3. Carrier lifetime prolongation of  $\alpha$ -FAPbI<sub>3</sub> upon compression.** **a**, pressure-dependent static PL signal in compression. The inset shows the red-shift of main peak position. **b-f**, *in-situ* high pressure dynamic PL measurements on a FAPbI<sub>3</sub> sample at 1 atm (**b**), 0.3 GPa (**c**), 0.8 GPa (**d**), 1.7 GPa (**e**), and 2.4 GPa (**f**). For all measured pressures, both slow ( $\tau_1$ ) and fast ( $\tau_2$ ) components of carrier lifetime were determined using biexponential fittings ( $I_{\text{PL}}(t) = I_{\text{int}}[\alpha \cdot \exp(-t/\tau_1) + \beta \cdot \exp(-t/\tau_2) + I_0]$ ) on time decay traces. **g**, pressure dependence relative changes in  $\tau_1$  and  $\tau_2$ . **h**, pressure dependence of the relative contribution of the bulk-dominated slow component,  $\alpha\tau_1/(\alpha\tau_1 + \beta\tau_2)$ . **i**, pressure dependence of the normalized mean carrier

lifetime,  $\langle\tau\rangle/\langle\tau\rangle_{(1\text{ atm})}$ , where  $\langle\tau\rangle=[\alpha\tau_1/(\alpha\tau_1+\beta\tau_2)]\tau_1+[\beta\tau_2/(\alpha\tau_1+\beta\tau_2)]\tau_2$ . Peak values in carrier lifetimes of FAPbI<sub>3</sub> were observed at 1.7 GPa, where a dramatic increase in  $\tau_1$  by 120% has been demonstrated. In **g-h**, the symbol size covers the size of the error bars.

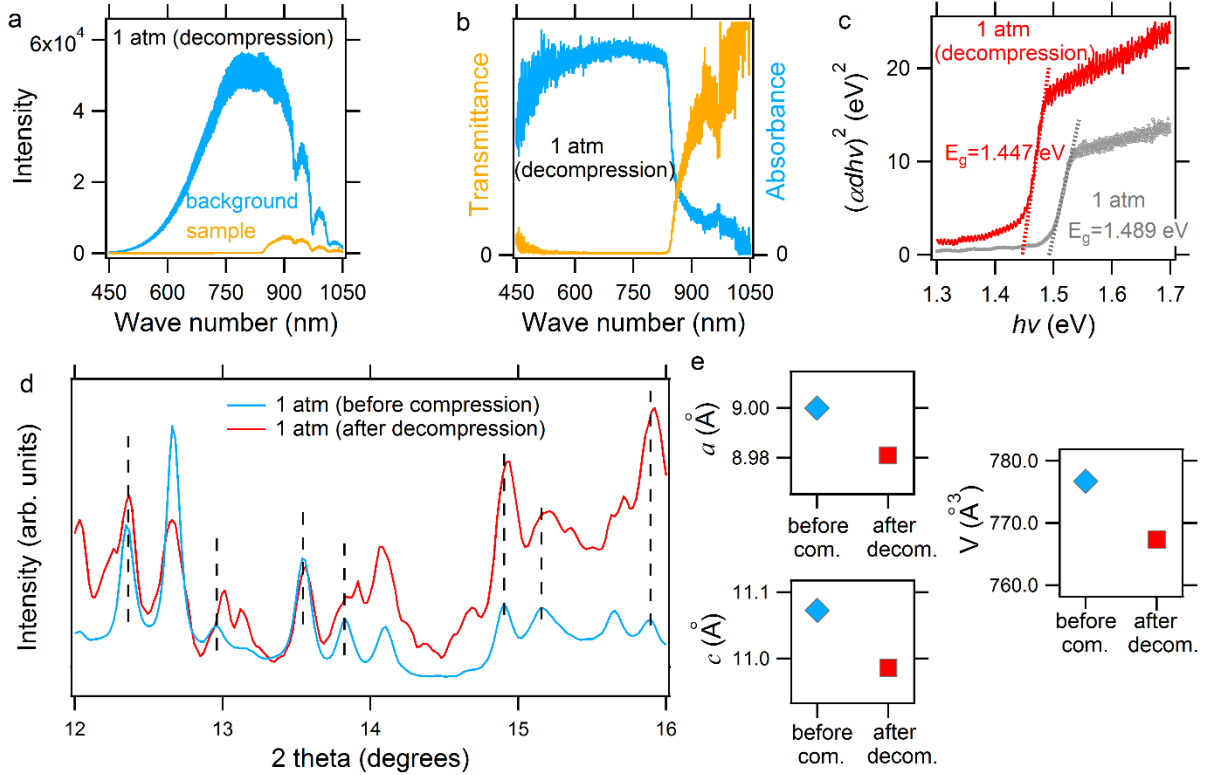


**Figure 4. Partial retainable bandgap observed in FAPbI<sub>3</sub>.** **a**, collected transmission spectra of the silicon oil background and FAPbI<sub>3</sub> sample (in the oil) after decompression back to 1 atm from 7.1 GPa. **b**, the absorbance and transmittance spectra of the decompressed sample were then obtained, and sharp absorbance (blue) and transmittance (orange) onsets are observed around 870 nm. **c**, Tauc plots for FAPbI<sub>3</sub> before compression (grey) and after decompression (red). Bandgap magnitudes were determined to be 1.489 eV before compression and 1.447 eV after decompression for FAPbI<sub>3</sub>. Such a ~42 meV decrease convinces the photonic retainability after applied pressure is totally released. **d**, comparison of powder X-ray diffraction pattern before compression (blue) and after decompression (red). Clearly, after decompression diffraction peaks shift toward higher 2 theta (lower d-spacing) range, demonstrating the quenched unit cell remembers some high pressure information. **e**, comparisons of lattice

parameters  $a$  (left upper),  $c$  (left lower) and cell volume (right) before compression and after decompression. The symbol size covers the size of the error bars.

## Methods

**Chemicals and reagents.** Hydriodic acid (HI, 57% w/w aqueous solution), lead(II) iodide ( $\text{PbI}_2$ , 99.9985% metals basis) and N,N-Dimethylformamide (DMF, anhydrous, 99.8%) were purchased from Alfa Aesar. Formamidine acetate (FAc, 99%) and  $\gamma$ -Butyrolactone (GBL,  $\geq 99\%$ ) were purchased from Aldrich. Lead acetate ( $\text{Pb}(\text{ac})_2 \cdot 3\text{H}_2\text{O}$ ) was purchased Mallinckrodt. Diethyl ether and acetonitrile (HPLC grade) were purchased from Fisher Chemical. All chemicals were used directly as received without further purification.

**Synthesis of FAI.** FAI was synthesized by drop-wise introducing 16.0 mL HI to 12.1130 g FAc in a 100-mL round bottom flask immersed in ice bath, with stirring in solution. FAc and HI were allowed to react for 12 h. The resulting solution was subsequently rotary evaporated at 60 °C until dry white-yellow solid formed. Collected solid was washed with diethyl ether and followed by vacuum filtration for 6 times. Pure compound was obtained by further drying in an oven at 110 °C for 12 hours.

**Synthesis of  $\text{FAPbI}_3$ .** 1:1 molar ratio of FAI and  $\text{PbI}_2$  were dissolved in DMF to make a 0.88 M perovskite solution. Precursor solution was heated at 80 °C with stirring for 1 hour, and then was hot-casted onto a pre-cleaned ZnSe substrate (Thorlabs). After the solvent evaporated, black  $\text{FAPbI}_3$  polycrystals were collected by carefully scraping down the glass slide using a plastic slide.  $\text{FAPbI}_3$  film was formed by annealing at 150 °C for 30 minutes for subsequent Infrared (IR) study.

**IR spectroscopy and mass spectrometry.** IR spectroscopy of  $\text{FAPbI}_3$  was acquired on a Nicolet IR spectrometer at Center for Nanoscale Materials, Argonne National Laboratory, and the result can be found in Supplementary Fig. S19. For mass spectrometry measurement, 1  $\mu\text{L}$  of as-prepared 0.88 M  $\text{FAPbI}_3$  precursor solution was diluted in DMF to make 10 mL of solution. FAI solution was prepared by dissolving 1 mg FAI in 60 mL acetonitrile. Each test solution was delivered into a Bruker Esquire 3000 Mass Spectrometer (Bruker Daltonics) through micro-syringe for spectrum measurement (see Supplementary Figs. S20-S24 and Supplementary Note 2).

***In-situ* synchrotron high pressure powder XRD.** *In-situ* synchrotron high pressure powder XRD experiments were carried out at 16-BM-D of the Advanced Photon Source (APS), Argonne National

Laboratory (ANL). Monochromatic X-ray with wavelength of 0.3066 Å was employed and the incident X-ray beam was focused to 4 μm × 5 μm spot. XRD patterns were collected with a MAR345 CCD detector. The samples were loaded in a symmetric type diamond anvil cell (DAC) with a pair of 300 μm culets and placed in a rhenium (Re) gasket hole with diameter of 140 μm drilled by a laser micro-matching system.<sup>38</sup> Silicon oil was used as pressure-transmitting medium. It should be noted that methanol/ethanol cannot be used as our organic-inorganic hybrid samples are easily decomposed in water and/or polar solvent.<sup>2</sup> Two ruby balls with diameters being on the order of 10 μm were loaded in the sample chamber. The pressure was determined by the ruby luminescence method. Such a pressure method was also employed in other high pressure experiments in this work, including high pressure optical absorbance measurement, and high pressure static photoluminescence and time-resolved photoluminescence dynamics experiment. GSAS program were employed to refine the obtained experimental XRD profiles.<sup>39</sup> Supplementary Fig. S25 shows the optical micrographs of FAPbI<sub>3</sub> in a diamond anvil cell at various pressures.

***In-situ* high pressure optical absorption spectroscopy.** *In-situ* high pressure optical absorption spectroscopy was conducted at the Infrared Lab of the National Synchrotron Light Source II (NSLS II) at Brookhaven National Laboratory (BNL). The visible absorption measurements between 10000 and 25000 cm<sup>-1</sup> utilized a customized visible microscope system.<sup>40</sup> A symmetric type diamond anvil cell (DAC) and a pair of IIA-type diamond anvils with the culets size of 300 μm were employed. Silicon oil was used as pressure transmitting medium and the silicon oil spectra were used to determine an absorbance baseline.

***In-situ* high pressure PL.** *In-situ* high pressure PL measurement was conducted at Center for Nanoscale Materials, Argonne National Laboratory. To measure static photoluminescence, FAPbI<sub>3</sub> samples were photoexcited at 450 nm and 40 nJ/cm<sup>2</sup> via a 35-ps pulsewidth laser diode. PL photons were collected with a lens and directed to a 300-mm focal-length grating spectrograph outfitted with a thermoelectrically cooled CCD and avalanche photodiode with time-correlated single-photon-counting electronics. The sample was loaded in Mao-type symmetric diamond anvil cell (DAC) with a pair of 300 μm culets and

placed in a rhenium (Re) gasket hole with diameter being on the order of 140  $\mu\text{m}$ . Silicon oil was used as pressure transmitting medium which provides good chemical inertness and hydrostatic condition.

38. Hrubciak, R., Sinogeikin, S., Rod, E. & Shen, G. The laser micro-machining system for diamond anvil cell experiments and general precision machining applications at the High Pressure Collaborative Access Team. *Rev. Sci. Instrum.* **86**, 072202 (2015).

39. Larson, A. C. & von Dreele, R. B. *General structure analysis system (GSAS)*. Los Alamos National Laboratory Report LAUR 86-748 (1994).

40. Jaffe, A., Lin, Y., Mao, W. L. & Karunadasa, H. I. Pressure-induced conductivity and yellow-to-black piezochromism in a Layered Cu–Cl Hybrid Perovskite. *J. Am. Chem. Soc.* **137**, 1673-1678 (2015).